

UNCLASSIFIED

AD NUMBER

AD819008

LIMITATION CHANGES

TO:

Approved for public release; distribution is unlimited.

FROM:

Distribution authorized to U.S. Gov't. agencies and their contractors; Critical Technology; JUN 1967. Other requests shall be referred to Naval Postgraduate School, Monterey, CA. This document contains export-controlled technical data.

AUTHORITY

usnps ltr, 6 oct 1971

THIS PAGE IS UNCLASSIFIED

AD819008

UNITED STATES
NAVAL POSTGRADUATE SCHOOL



THESIS

THE PRODUCTION OF Be^7 AND C^{11} FROM CARBON,
NITROGEN, AND OXYGEN BY 75-MeV ELECTRONS

by

James Allen Lusk

and

Glenn Waldo Pomykal

This document is subject to special export controls and each transmittal to foreign government or foreign nationals may be made only with prior approval of the U. S. Naval Postgraduate School.

THE PRODUCTION OF Be^7 AND C^{11} FROM CARBON,
NITROGEN, AND OXYGEN BY 75-MEV ELECTRONS

by

James Allen Lusk
Major, United States Army
B.S., University of Nevada, 1957

and

Glenn Waldo Pomykal
Lieutenant, United States Navy
B. A., The Agricultural and Mechanical College of Texas, 1962

Submitted in partial fulfillment of the
requirements for the degree of

MASTER OF SCIENCE IN PHYSICS

from the

NAVAL POSTGRADUATE SCHOOL
June 1967

Signature of Author(s)

James A. Lusk

Glenn W. Pomykal

Approved by

Harvey A. Dall

Thesis Advisor

E. C. Brittenden, Jr.

Chairman, Department of Physics

R. F. Pinchart

Academic Dean

ABSTRACT

An investigation was made of the electromagnetic disintegration of carbon, nitrogen, and oxygen leading to production of the unstable nuclei Be^7 and C^{11} . Targets of graphite, melamine, and water were bombarded with 75-MeV electrons from the Naval Postgraduate School linear accelerator. The disintegration fragments of interest were counted by detecting their decay activity, Be^7 by the 477-Kev gamma ray from its daughter nucleus and C^{11} by the 511-Kev photons from the annihilation of its emitted positron. Electron and photon effects were separated by interposing an additional radiator for one bombardment of a given type of target, then repeating with a similar target without the radiator.

Radioactive fragments of Be^7 and C^{11} were found in all bombardments; N^{13} was also found in bombardments of melamine and water. Electrodisintegration cross sections for processes yielding C^{11} were found to range from $17.5 \mu\text{b}$ for carbon down to $0.3 \mu\text{b}$ for oxygen. The corresponding values for processes yielding Be^7 ranged from $1.3 \mu\text{b}$ to $0.14 \mu\text{b}$. Integrated photodisintegration cross sections were found to be approximately 50 times greater than these.

TABLE OF CONTENTS

Chapter	Page
I. Introduction	9
II. Experimental Details	12
A. The Accelerator System	12
B. Monitoring of the Primary Beam	12
C. Target Configuration	13
D. Bremsstrahlung Production	14
E. Detection System	17
III. Data Reduction	24
A. Yield of Radioactive Nuclei	24
B. Derivation of Cross Section Equations	25
C. Bremsstrahlung Spectrum	29
D. Equivalent Radiator Thickness	31
E. Calculations for Nitrogen	33
F. Radionuclide Identification	34
G. Efficiency of Counting	37
H. Calculations of the Activity	38
I. Error Analysis	39
IV. Results	41
Bibliography	46
Appendix I	47
Appendix II	51

LIST OF TABLES

I.	Radiating Material Thickness	16
II.	Experimental Data	41
III.	Total Cross Section for Formation of C^{11}	42
IV.	Total Cross Section for Formation of Be^7	42
V.	Total Cross Section for Formation of N^{13}	43
VI.	Equivalent Radiator Thicknesses	44
VII.	Detector Efficiency	53

LIST OF ILLUSTRATIONS

1.	Melamine Target Details	15
2.	Water Target Details	15
3.	Geometry for Counting	18
4.	Block Diagram of Counting Circuits	20
5.	Cs ¹³⁷ Pulse-Height Spectrum	21
6.	Plot of Counts Vs Gain	21
7.	Bremsstrahlung Intensity Spectrum	32
8.	C ¹¹ Pulse-Height Spectrum	35
9.	Be ⁷ Pulse-Height Spectrum	36
10.	Photomultiplier Tube Base Circuit	48
11.	Channel Advance Trigger Circuit	50

I. INTRODUCTION

The investigation of nuclear structure is generally accomplished by permitting energetic radiation from some external source to interact with, and perhaps to disintegrate, the nucleus in question. Analysis of the distribution of the resulting fragments can lead to information concerning both the original structure of the target nucleus and the specific interaction mechanisms involved. If the projectile particle is of a nuclear sort, separation of the two types of information will be very difficult due to our incomplete understanding of specifically nuclear interactions. If, however, the primary radiation is of electromagnetic nature, as in the experiment to be reported here, we believe the interaction process to be fairly well understood. Direct information can then be obtained about the structure of the original nucleus alone, providing only that the energy and angle distributions of all disintegration fragments can be determined.

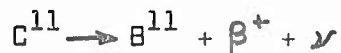
Measurements of the distributions of individual light charged particles (proton, deuterons, alpha particles) or of neutrons resulting from photodisintegration or electrodisintegration processes have been accomplished by many experimental groups [1,2] over the last thirty years. On the other hand, experimental information on the distributions of all of the emitted fragments from a given disintegration is relatively sparse, being restricted mainly to experiments in which the disintegrations occurred in nuclear emulsions [3]. The difficulty of measuring all the fragments in an experiment using counters is somewhat greater, both because coincidence techniques are required, and because the heavy

fragments cannot escape from any but the thinnest of targets. As a first step in obtaining information concerning the processes which result in heavy disintegration fragments, several experimental groups [4,5] have measured the end-product radioactivity following bombardment of selected nuclei. The total cross section for production of unstable nuclei as disintegration fragments is relatively easily obtained. It constitutes one of the bits of information from which complete knowledge of the angle and energy distributions of all the emitted products may some day be pieced.

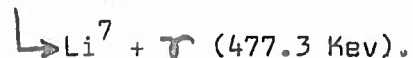
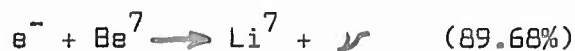
In an effort to obtain information about electromagnetic interactions with light nuclei, we conducted an experiment at the Naval Postgraduate School to measure the total cross sections for the photodisintegration and electrodisintegration of carbon, nitrogen, and oxygen in processes leading to the radioactive fragments C^{11} and Be^7 . Aside from the theoretical interest that attaches to interactions with light nuclei, these elements were selected for study on the basis of certain practical considerations. Each occurs in shielding materials used in the target areas of accelerators and thus constitutes a radioactive source when activated by a high-intensity electron beam. The resulting radiation can be hazardous if the target area must be entered before the radiation has had an opportunity to decay to a safe level. It was our intention to measure the relevant production cross sections in order to determine how rapidly such hazardous long-lived activity is built up.

Interactions which lead to the fragments Be^7 or C^{11} may occur in a great variety of forms. As examples of possible photodisintegration processes occurring in the experiment, we might list

$O^{16}(\gamma, \alpha n)C^{11}$, $C^{12}(\gamma, n)C^{11}$, $O^{16}(\gamma, 2\alpha n)Be^7$, $N^{14}(\gamma, Li^7)Be^7$, or $C^{12}(\gamma, \alpha n)Be^7$. If one replaced the photon by an electron (which scatters in the interaction), these expressions would also display valid examples of electrodisintegration processes. In any event, the disintegration cross sections can be measured if one detects the radiations emitted in the decay of the heavy fragment. For example, the product nuclei C^{11} and N^{13} decay by positron emission, as shown by the equations



Following its emission the positron annihilates with an electron; this leads to the appearance of two 511-Kev photons which may be detected. Similarly, the heavy fragment Be^7 decays by electron capture to the final nucleus Li^7 according to one of the equations.



One notes that in 10.32 percent of the decays the Li^7 daughter nucleus is left in an excited state. The 477.3-Kev gamma ray which results in the subsequent de-excitation of Li^{7*} provides one with a means of determining the number of Be^7 nuclei that were produced in the primary disintegration.

II. EXPERIMENTAL DETAILS

A. The Accelerator System

The source of the high-energy electrons for this experiment was the 120-MeV linear accelerator at the Naval Postgraduate School. This machine provided primary electrons with an energy of 75 MeV and an intensity of 5×10^{12} electrons per second in a beam with diameter of about 3/8-inch at the collimator. After the collimator the electrons entered the first deflection magnet and were deflected through 30 degrees from the accelerator axis. In this way the neutrons and bremsstrahlung photons produced in the accelerating structure could be removed from the electron beam. The deflecting magnet and the energy slits following it determine the primary electron energy. The energy slit width defines the uncertainty in the electron energy; in our experiment this uncertainty was ± 1 percent. Following the slits, the beam finally passed through the focusing magnet which bent it another 30 degrees into the experimental area, in which the bombardments occurred.

B. Monitoring of the Primary Beam

A secondary-electron-emission monitor was installed at the end of the beam tube, after the focusing magnet, but ahead of the target assembly. The current produced in this 5-foil monitor was permitted to charge a capacitor of known capacitance. Measurement of the capacitor voltage by means of an integrator circuit then enabled us to determine the total electron charge that had passed through the monitor and into the target. The monitor has an efficiency of 0.05 and an accuracy of 10 percent. Fluctuations

in beam intensity were not recorded. We did, however, note the periods in which the beam failed entirely. During the actual "on" periods the average beam current was assumed to be constant. This assumption leads to some error in results for the short-lived C^{11} product nuclei.

During bombardment the electron beam was visually observed by use of remote television. A ZnS screen was placed in front of each target. The beam spot produced on this screen was observed by the operator as a means of steering the beam and focusing it on the center of the target.

C. Target Configuration

Nuclei of the elements carbon, nitrogen, and oxygen were of interest as targets in this experiment. The carbon targets were made of spectral grade graphite* of 99.9% purity, 1.586 g/cm^3 density, machined into discs of 0.973-inch diameter and 0.200-inch thickness. During irradiation the electron beam was incident on each disc along its axis of symmetry.

The nitrogen nuclei were bombarded in a target of melamine, $C_3H_6N_6$, an organic compound with molecular weight 126.1 grams per mole. The target material was in the physical form of a fine crystalline powder of density 1.107 g/cm^3 and 97 percent purity.** The melamine was tightly packed into an aluminum alloy (type 6061) container which held the powder in an 0.866-inch diameter by

* Manufactured by Union Carbide Corp., Carbon Products Div., New York, N.Y.

** Manufactured by Eastman Organic Chemicals, Rochester, N.Y.

0.200-inch thick configuration. The samples were irradiated with the discs coaxial with the beam centerline (Fig. 1). Each target was cooled to prevent melting or sublimation of the material.

Oxygen nuclei were bombarded in a target of distilled water enclosed in an aluminum alloy (type 6061) holder which contained the water in a configuration 0.75 inches wide, 0.75 inches high, and 0.26 inches thick in the direction of the electron beam (Fig. 2). The water was not degassed prior to irradiation. It was cooled during irradiation to prevent vaporization.

In order to cool the melamine and water, these target holders were mounted on an aluminum support which was part of the moveable target frame. The base of the support was inserted in an insulated flask filled with liquid nitrogen. Thus the heat generated in the target by the electron bombardment was conducted downwards and dissipated in the liquid nitrogen. There was no apparent loss of melamine or water during irradiation.

D. Bremsstrahlung Production

Accompanying the electron beam in the target area of a linear accelerator are some unavoidable bremsstrahlung photons. These are produced in all material through which the high-energy electrons pass, including the target itself. In our experiment the following items were present as bremsstrahlung producers in all irradiations: the window of the electron beam tube and the foils of the secondary-emission monitor, 0.152 mm of aluminum; an aluminum foil target for a simultaneous experiment, 0.118 mm; the air between the end of the vacuum pipe and the target, 63.5 cm; a ZnS layer, 0.061 mm, deposited on an aluminum foil, 0.058 mm.

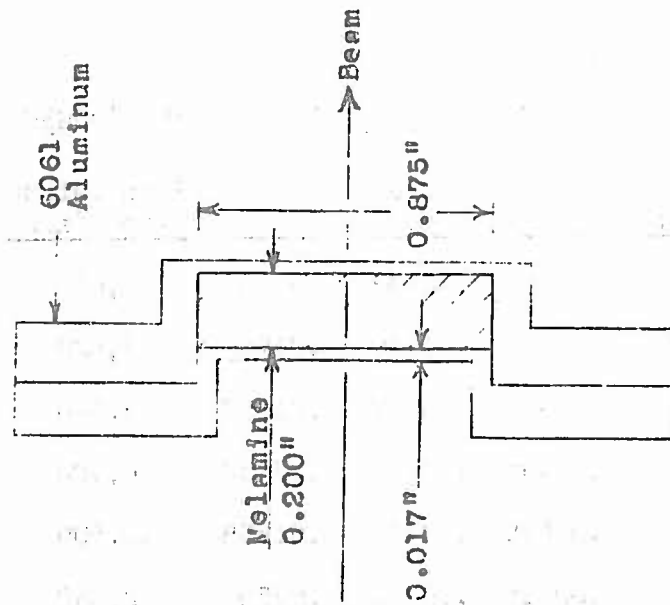


Fig. 1 Melamine Target Details

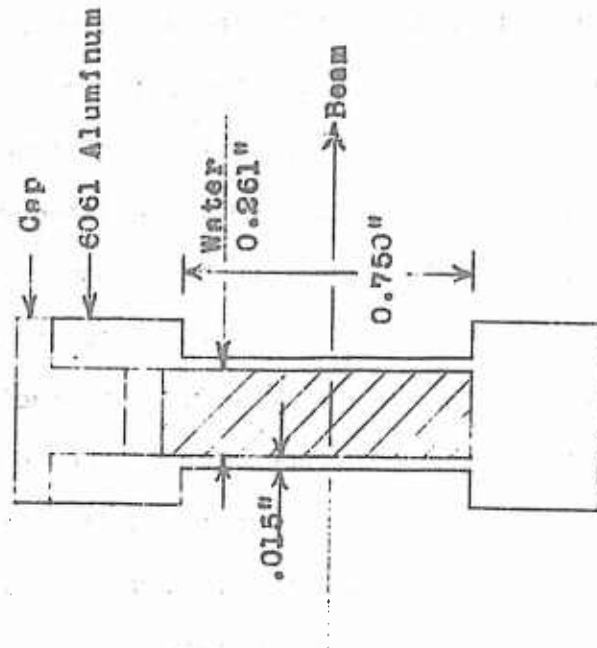


Fig. 2 Water Target Details

change the water target. The target is also used for the water target and is also used for the water target.

The water and melamine targets contributed additional material in front of the actual target material. The upstream walls of the holders were 0.367 and 0.438 mm, respectively, of type 6061 aluminum alloy. This is composed of 1.0 percent magnesium, 0.6 percent silicon, and 0.25 percent each of copper and chromium, alloyed with aluminum. The radiation thicknesses of the holders are reported in the third column of Table I. The radiation thickness of half the target itself is tabulated in the fourth column. For all samples irradiated with the copper radiator "in" a sheet of oxygen-free, high-conductivity copper, 0.792 mm thick, was mounted directly in front of the appropriate target. This interposed an additional 0.0550 radiation lengths of material.

TABLE I
Radiating Material Thickness

All thicknesses are in units of radiation lengths

Sample	Extra Radiator	Target Wall	Target Body	Total	Irradiation Time (sec)	Total Charge (μ coul)
Carbon 1	in	-	.00939	.07189	4,680	248
Carbon 2	out	-	.00939	.01694	7,620	314
Carbon 3	out	-	.00939	.01693	9,540	433
Mel. 1	in	.00495	.00687	.07432	6,900	401
Mel. 2	out	.00495	.00713	.01958	10,500	413
Water 1	in	.00415	.00922	.07587	12,840	521
Water 2	out	.00415	.00922	.02087	11,790	561

Table I also lists total irradiation time and accumulated charge for each sample. The carbon-2 and water-2 samples had

"beam off" intervals during their irradiation. These interruptions were, of course, taken into account in the calculation of the cross sections for the nuclei involved in these samples. The method for doing this will be discussed in Chapter III.

E. Detection System

After bombardment, each sample was removed from its holder and placed in a polyethylene bottle with an inside diameter of 0.980 inches and a 0.047-inch wall thickness. Each bottle was then sealed with epoxy resin to prevent spillage or evaporation of the sample, or contamination of the counter house. In the water bombardments, however, an additional step was taken. Crystals of BeNO_3 were added to the water sample, prior to its removal from the target holder. This causes an exchange between the Be^9 ions and the radioactive Be^7 adsorbed to the container walls and allows a more complete transfer of Be^7 into the bottle.

The counter-house was constructed of standard 2x4x8-inch lead bricks which were stacked to form a base, walls, and top each of 6-inch thickness. The inside well was 20x20 inches by 24 inches high. An 8x8-inch access port in the top was covered during counting by a 6-inch lead cap. The scintillation crystal-photo-multiplier tube was mounted in a holder centered on the base of the counter-house well with the crystal face pointing upward at a height of 11.5 inches above the bottom of the well (Fig. 3). The holder which fixed the position of the sample bottle during counting was fabricated of 1/8-inch lucite sheet supported by three lucite rods. This assembly was placed over the counter in

-equivalent to the...
 design...
 lead...

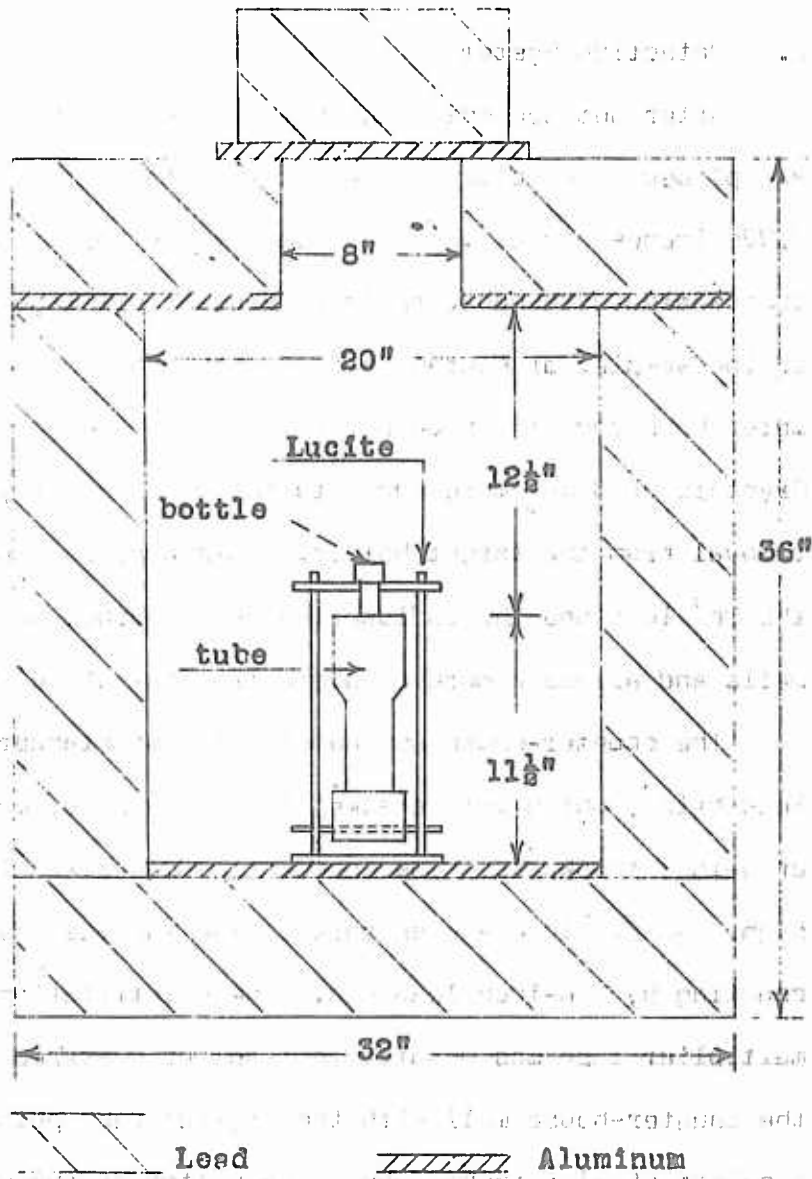


Fig. 3 Geometry for Counting

such a way that the base of the sample bottle came nearly in contact with the tube face, providing the maximum counting efficiency.

The electrical equipment associated with the experiment is shown in a block diagram in Fig. 4. The counter used was a Harshaw Type 12S12 "Integral Line" Assembly which employs a cylindrical NaI(Tl) crystal 3 inches in diameter and 3 inches long coupled to an RCA type 8054 photomultiplier tube. The remainder of the electronic apparatus and the photomultiplier tube base circuit are discussed in Appendix 1.

Preliminary experiments, not here reported, established a requirement for close scrutiny of the gain and voltage stability of the system. A reliable method of minimizing the effects of troublesome gain shifts was finally achieved using the essentially constant activity of a Cs¹³⁷ source. The source, a small amount of CsCl on a copper disc, was mounted in a holder that enabled it to be placed in the same identical spot over the counter for each calibration.

The amplifier gain-setting procedure was then determined as follows. The tube high-voltage being set at 1100 volts, the amplifier gain was adjusted so that the 662-Kev photopeak maximum of the cesium spectrum fell in channel 339 of the 512-channel pulse-height analyzer. With the internal gain of the analyzer already properly adjusted at this point, the 32-Kev barium x-ray line then fell in channel 16, as shown in Fig. 5. Pulses from a mercury-switch pulser were then applied at the amplifier input terminals. The pulse amplitude was adjusted so that the amplifier output pulses would fall into channel 320, at about half-maximum

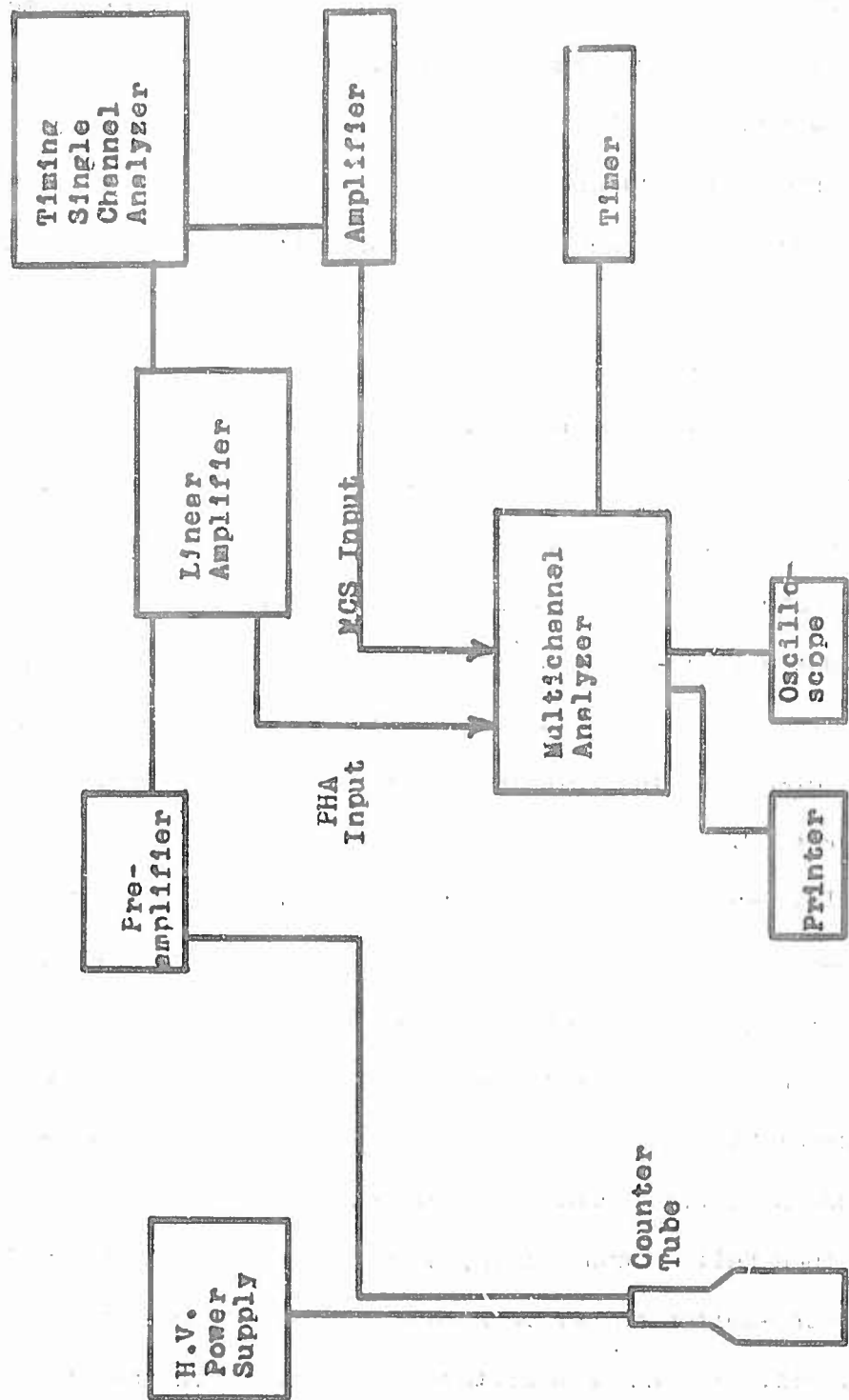


Fig. 4 Block Diagram of Counting Circuits

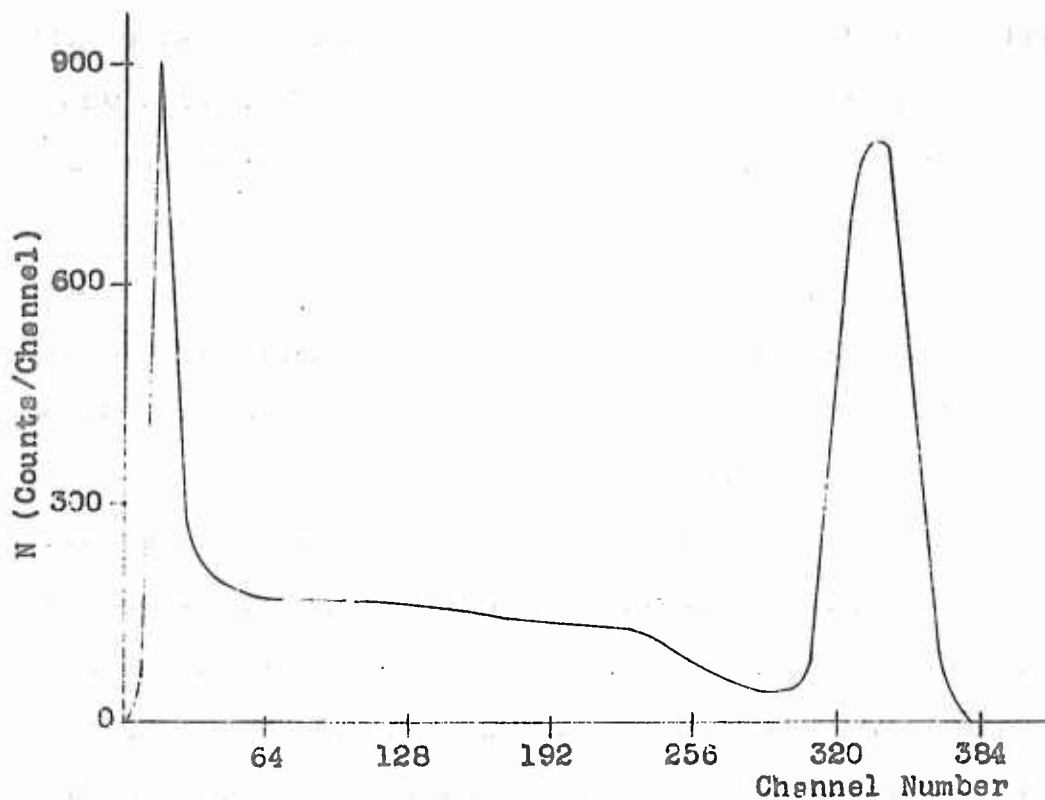


Fig. 5 Cs^{137} Pulse-Height Spectrum

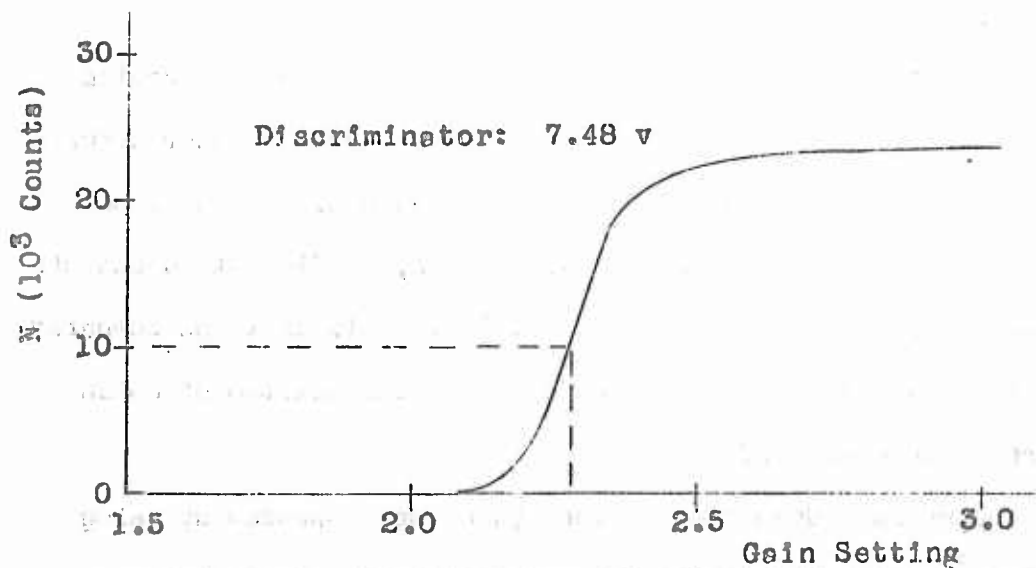


Fig. 6 Plot of Counts vs Gain Setting

on the low-voltage edge of the cesium photopeak. The integral discriminator of the single channel analyzer was then set to just cut off the pulses that would fall into channel 320. With this discriminator setting, 7.48 volts, and with the analyzer in the multi-channel scaling mode, the cesium activity was measured to be very nearly 10,000 counts in 16 2/3 seconds when the gain was at the desired level. Small variations of the amplifier gain or counter high-voltage, on the other hand, would cause large changes in counting rate from the cesium calibration source.

The technique for subsequent gain settings was very simple. The cesium calibration source was put into position, the discriminator was set at 7.48 volts, and the high-voltage was set at 1100 volts. The amplifier gain was then adjusted until 10,000 counts appeared in 16 2/3 seconds. In this way the gain of the system was fixed relative to the discriminator setting. The sensitivity of the technique can be seen from the slope of the gain curve shown in Fig. 6.

Since the Be^7 or C^{11} radiations occur with lower energies than those from Cs^{137} , it was necessary to choose a lower discriminator setting when detecting these radiations. For this we used a discriminator setting of 4.50 volts, sufficient to cut off pulses in all channels below channel 192. This is to be compared with the position of the 477-Kev Be^7 peak the maximum of which occurs in channel 241.

The overall dead time of the system was measured by using two Cs^{137} sources of nearly equal intensity and following the technique known as the two-source method. The dead time was

found to be 2.38 microseconds for the multichannel-scaling mode of the pulse height analyzer and for a minimum discriminator setting giving a cutoff at about zero Kev.

III. DATA REDUCTION

A. Yield of Radioactive Nuclei

In the course of the bombardment of a given target, radioactive fragments were produced either by real photons or by the electrons themselves interacting with the original nuclei. To enable us to determine the cross section for each of these processes separately, we irradiated two samples of each type, one with a copper radiator in advance of the target, the other without the radiator. By performing a subtraction of one result from the other, we were thus able to separate the photon and electron effects.

Consider the number of radioactive nuclei produced in a target by the bremsstrahlung from an electron which has passed through one radiation length of material. Suppose that the resulting photons then fall on a target of one atom per unit area, producing a certain number of radioactive fragments (one per interaction). This number, the so-called photoyield, is given by the expression

$$Y_T(E_0) = \int_{E_{th}}^{E_0} \sigma_T(k) \Phi(E_0, Z, k) dk. \quad (1)$$

Here $\sigma_T(k)$ and E_{th} are respectively the cross section and threshold energy for the photodisintegration process, and $\Phi(E_0, Z, k)dk$ is the bremsstrahlung number spectrum. This gives the number of photons of energy between k and $k+dk$ produced in one radiation length of material. The bremsstrahlung spectrum will be discussed in detail in section C of this chapter.

The yield of radioactive nuclei produced in a target of one atom per unit area by the electromagnetic field of the electron itself is seen to be numerically equal to the electrodisintegration cross section. This gives the equality

$$Y_e(E_0) = \sigma_e(E_0) \quad (2)$$

in which E_0 is the electron energy. One notes that the right side is implicitly multiplied by $N=1$ atom per unit area in order that the equation may have dimensional consistency.

B. Derivation of Cross Section Equations

The rate of change of the number of radioactive nuclei in a target during irradiation is seen to be

$$\frac{dn}{dt} = NT \left[\sigma_e(E_0) + X \int_{E_{th}}^{E_0} \sigma_r(E_0) \Phi(E_0, z, k) dk \right] I(t) - \lambda n, \quad (3)$$

in which the square bracket term is the rate of production and the last term, $-\lambda n$, is the rate of decay of the produced fragments. In the above equation λ is the decay constant of the radioactive nuclei, n is the number of radioactive nuclei present at any one time, $I(t)$ is the intensity in electrons per second of the electron beam as a function of time, N is the number of atoms per cubic centimeter of the target, and T is the target thickness in centimeters. Rewriting equation (3) by using the definitions of equations (1) and (2), one obtains the equation

$$\frac{dn}{dt} + \lambda n = NT \left[Y_e(E_0) + X Y_r(E_0) \right] I(t). \quad (4)$$

The term $XY_{\gamma}(E_0)$ on the right side of equation (4) should actually be represented by the sum

$$XY_{\gamma}(E_0) = \sum_i X_i Y_{\gamma i}(E_0) \quad (5)$$

to allow for slightly differing shapes of the bremsstrahlung spectra $\Phi(E_0, Z, k)$ arising from the different radiating materials in the beam. However, the two extreme examples of radiator materials used in the experiment, hydrogen and copper, have photon spectra differing by ten percent at most. We can thus take the photoyield integral for copper to be appropriate for the yields due to photons from other radiators as well. The total error in doing this will be considerably less than ten percent when the cross section is properly folded in. The right side of equation (5) then reduces to a sum over radiation thicknesses multiplying the photoyield due to photons from copper. In what follows we shall take X to be a sum over radiation thicknesses of all the material in the beam; Y_{γ} shall be the photoyield appropriate to copper.

Multiplying equation (4) by the integrating factor $e^{\lambda t}$ and integrating over time, we obtain the number of radioactive nuclei present at the time τ at which the irradiation ceased,

$$n(\tau) = NT \left[Y_0(E_0) + XY_{\gamma}(E_0) \right] \int_0^{\tau} I(t) e^{-\lambda(\tau-t)} dt \quad (6)$$

If the nucleus decays by one mode only, the activity at time τ will be

$$A(\tau) \equiv A_0 = \lambda n(\tau) \quad (7)$$

or

$$A_0 = \lambda NT [Y_e(E_0) + X Y_r(E_0)] \int_0^{\tau} I(t) e^{-\lambda(\tau-t)} dt. \quad (8)$$

We next define the total yield per electron for a beam passing through material of total thickness X radiation lengths followed by a target composed of one atom per unit area by the equation

$$Y_e(E_0) + X Y_r(E_0) = \frac{A_0}{\lambda NT \int_0^{\tau} I(t) e^{-\lambda(\tau-t)} dt} \equiv R. \quad (9)$$

The total yield is now in terms only of quantities which can be measured directly in the laboratory. Suppose we let the radiation thickness of the copper radiator be X_r and that of all the other material be X_j . The total yield for the irradiation made with the additional radiator in place is then

$$Y_e(E_0) + (X_j + X_r) Y_r(E_0) = R_1. \quad (10)$$

Without the radiator the total yield is

$$Y_e(E_0) + X_j Y_r(E_0) = R_2. \quad (11)$$

The symbols R_1 and R_2 represent the right side of equation (9) with the appropriate experimental quantities substituted. Subtracting equation (11) from equation (10) one obtains

$$X_r Y_r(E_0) = R_1 - R_2. \quad (12)$$

Ideally, one would now return to equation (1) and solve for $\sigma_r(k)$. This is, however, not entirely feasible at this point. To solve for $\sigma_r(k)$ requires the unfolding of the bremsstrahlung spectrum to determine exactly which photon produced what interaction. This is a time-consuming procedure at best and was not attempted in view of the limited time available to us. Instead, we computed an average cross section, $\sigma_a(E_0)$, which is defined from

$$\sigma_a(E_0) = \frac{E_0 \int_{E_{th}}^{E_0} \sigma_r(k) \Phi(E_0, z, k) dk}{\int_0^{E_0} k \Phi(E_0, z, k) dk} \quad (13)$$

In equation (13) the denominator represents the average bremsstrahlung energy produced when an electron passes through one radiation length of material. When the denominator is divided by E_0 it provides an "equivalent number" of photons of energy E_0 produced per radiation length. Using equation (1) and (12), one obtains finally

$$\sigma_a(E_0) = \frac{E_0 (R_1 - R_2)}{X_r \int_0^{E_0} k \Phi(E_0, z, k) dk} \quad (14)$$

Equation (14) states the photodisintegration cross section per equivalent photon in terms of measured quantities.

The electrodisintegration cross section, $\sigma_e(E_0)$, can also be calculated from the experimental yields R_1 and R_2 . By using

equations (11) and (12) one obtains the expression

$$\sigma_e(E_0) \equiv Y_e(E_0) = R_2 - \frac{X_i}{X_r} (R_1 - R_2). \quad (15)$$

The right side of this equation is stated in terms only of measurable quantities.

C. Bremsstrahlung Spectrum

In our investigation of the photodisintegration process, we produced a known amount of bremsstrahlung by placing radiators of given thickness in the electron beam. Although a little of the radiating material was as much as sixty centimeters from the target, the greater portion was in close proximity to it. It thus seems to us that essentially all of the bremsstrahlung produced passed through the target. That this is a reasonable assumption may be seen from the discussion by Heitler [6]. This shows that the mean angle of emission of bremsstrahlung is of the order $\frac{m_0 c^2}{E_0}$ radians with respect to the beam direction. In our case this is an angle of 0.39 degrees. Clearly, most of the radiation is very nearly in the forward direction.

In calculating the photon spectrum we used the differential bremsstrahlung cross section $\frac{d\sigma_{\text{rad}}}{dk}$ obtained from the paper of Koch and Motz [7], but modified to include the scattering effect of the atomic electrons. We used two different forms of these equations, appropriate for two separate regions of values of the screening parameter γ defined by the expression

$$\gamma = \frac{100 m_0 c^2 k}{E E_0 Z^{1/2}} \quad (16)$$

The relationship between the Koch and Motz differential cross sections and our bremsstrahlung number spectrum $\Phi(E_0, Z, k)$ may now be written in the combined form

$$\frac{d\sigma_{rad}}{dk} = \left[\frac{4Z(Z+\xi)r_0^2}{137} \ln(183Z^{-1/3}) \right] \Phi(E_0, Z, k). \quad (17)$$

Here the function $\Phi(E_0, Z, k)$ has the form, for $0 < \gamma < 2$;

$$\Phi(E_0, Z, k) = \frac{1}{k \ln(183Z^{-1/3})} \left\{ \left(1 + \frac{E^2}{E_0^2}\right) \left[\frac{\phi_1(\gamma)}{4} - \frac{\ln Z}{3} \right] - \frac{2E}{3E_0} \left[\frac{\phi_2(\gamma)}{4} - \frac{\ln Z}{3} \right] \right\} \quad (18)$$

or, for $2 < \gamma < 15$,

$$\Phi(E_0, Z, k) = \frac{1}{k \ln(183Z^{-1/3})} \left\{ \left[1 + \frac{E^2}{E_0^2} - \frac{2E}{3E_0} \right] \left[\ln \left(\frac{2EE_0}{km_0c^2} \right) - \frac{1}{2} - c(\gamma) \right] \right\} \quad (19)$$

In the above equations ξ is a parameter by means of which bremsstrahlung produced off the atomic electrons is included. The other quantities are the classical electron radius, $r_0 = e^2/m_0c^2$, and the final energy of the scattered electron, $E = E_0 - k$. Values of the functions $\phi_1(\gamma)$, $\phi_2(\gamma)$, and $c(\gamma)$ were taken from graphs in reference [7].

We note that the radiation length of a material of atomic number Z , atomic weight A , is

$$X_0 = \frac{137A}{4N_0Z(Z+\xi)r_0^2 \ln(183Z^{-1/3})} \quad (20)$$

The cross section for bremsstrahlung production is then found from equation (17) to be

$$\frac{d\sigma_{\text{rad}}}{dk} = \frac{1}{X_0} \frac{A}{N_0} \Phi(E_0, Z, k) \quad (21)$$

When an electron of energy E_0 passes through a radiator of thickness T , composed of N atoms per unit volume, the number of photons produced with energy between k and $k+dk$ will be

$$NT \frac{d\sigma_{\text{rad}}}{dk} dk = X \Phi(E_0, Z, k) dk \quad (22)$$

Here we have put $N = \rho N_0/A$ and $X = \rho T/X_0$, the latter being the radiator thickness in units of radiation lengths. In all the calculations we used values of the radiation lengths X_0 given by Bethe and Ashkin [8]. The values of X_0 used for the principal radiators were as follows: 58 for H, 42.5 for C, 23.9 for Al, 12.8 for Cu, 36.5 for air, all numbers in units of g/cm^2 .

Figure 7 shows the intensity spectrum, $k\Phi(E_0, Z, k)$, for bremsstrahlung from copper and carbon.

D. Equivalent Radiator Thickness

Another quantity of interest in an experiment using electrons as projectiles is the equivalent radiator thickness, designated as X_e radiation lengths. This is defined as the thickness of radiator material necessary to produce real photons in sufficient quantity to give the same disintegration yield in the target as that produced by the electrons themselves. The quantity X_e pro-

The cross-section for bremsstrahlung is given by the following formula:

$$\sigma_{br} = \frac{16}{3} \frac{Z^2 r_e^2}{\pi} \ln \left(\frac{2\gamma - 1}{\gamma - 1} \right) \frac{1}{\gamma} \left(\frac{Z}{137} \right)^2$$

where γ is the relativistic factor, Z is the atomic number, and r_e is the classical electron radius.

The intensity of bremsstrahlung is proportional to the cross-section and the number of electrons.

$$I_{br} \propto Z^2 \ln \left(\frac{2\gamma - 1}{\gamma - 1} \right) \frac{1}{\gamma} \left(\frac{Z}{137} \right)^2$$

For a given energy, the intensity is higher for a material with a higher atomic number.

The following table shows the relative intensity of bremsstrahlung for different materials.

Material	Relative Intensity
Copper	1.0
Carbon	0.1

As shown in the graph, the intensity of bremsstrahlung increases rapidly with energy and is much higher for copper than for carbon.

The graph shows the intensity of bremsstrahlung for copper and carbon as a function of photon energy.

The y-axis represents the intensity $k(R_0, Z, k)$ and the x-axis represents the photon energy k in MeV.

The curve for copper is significantly higher than the curve for carbon, indicating a much higher intensity of bremsstrahlung for copper at any given energy.

The intensity increases with energy and levels off at high energies.

The following table shows the intensity of bremsstrahlung for copper and carbon at various photon energies.

Photon Energy k (MeV)	Intensity $k(R_0, Z, k)$ (Copper)	Intensity $k(R_0, Z, k)$ (Carbon)
0	0	0
10	~1.0	~0.1
20	~1.8	~0.2
30	~2.5	~0.3
40	~3.0	~0.4
50	~3.5	~0.5
60	~3.8	~0.55
70	~4.0	~0.6
80	~4.1	~0.6

Fig. 7 Bremsstrahlung Intensity Spectrum

vides a convenient parameter useful in comparing the disintegration effects of the virtual photons of the electron field with the effects of real bremsstrahlung photons.

Using the equivalent radiator thickness, one may define the yield from electrodisintegration to be

$$Y_e(E_0) = X_e \int_{E_{th}}^{E_0} \sigma_T(k) \Phi(E_0, Z, k) dk. \quad (23)$$

This is identical with equation (1) except for the presence of the factor X_e . Using this definition, along with equations (11) and (12), one obtains the equivalent thickness,

$$X_e = \frac{R_2}{R_1 - R_2} X_T - X_j \quad (24)$$

stated in terms only of measurable quantities.

E. Calculations for Nitrogen

Melamine contains both carbon and nitrogen, each of which contributes Be^7 or C^{11} disintegration fragments. The calculation of the nitrogen disintegration cross sections from measured melamine yields thus requires the subtraction of the carbon effects. We define a disintegration cross section for the melamine molecule as a sum of the cross sections of its constituent atoms. From this we find the nitrogen cross section, applicable in form for either photodisintegration or electrodisintegration, to be

$$\sigma_N = \frac{1}{6} (\sigma_{\text{mel}} - 3\sigma_C). \quad (25)$$

The melamine and carbon cross sections, σ_{Mel} and σ_{C} , respectively, are to be obtained either from equation (14) or from equation (15) and the appropriate measured quantities.

F. Radionuclide Identification

The two primary radionuclides of interest in this experiment, Be^7 and C^{11} , and a third which was observed, N^{13} , were identified by means of both energy-spectrum and half-life measurements. For each sample a first pulse-height analysis was made during the early stages of decay when C^{11} and, in the case of the water, N^{13} were the prevalent radionuclides decaying. At this point the spectrum was scanned for evidence of other radiations besides the 511-Kev positron-annihilation photons or the 477-Kev Li^7 gamma rays. In no case were other radiations present in sufficient quantity to be observed. A typical pulse height spectrum is given in Fig. 8, which shows the annihilation photon peak from the C^{11} decays in a typical carbon sample.

The second and subsequent pulse-height analyses were made for each sample at a later time when the only decay observed was that of Be^7 , which produced 477-Kev quanta. An example of this is shown in Fig. 9, which displays the Be^7 decay spectrum for a water sample.

The N^{13} decays were observed in the water samples but not in the melamine. The seeming absence of N^{13} in melamine was incurred by necessary delays in the counting of these samples. The C^{11} activity in the melamine was sufficient to saturate the counter system. After this had abated sufficiently to enable us

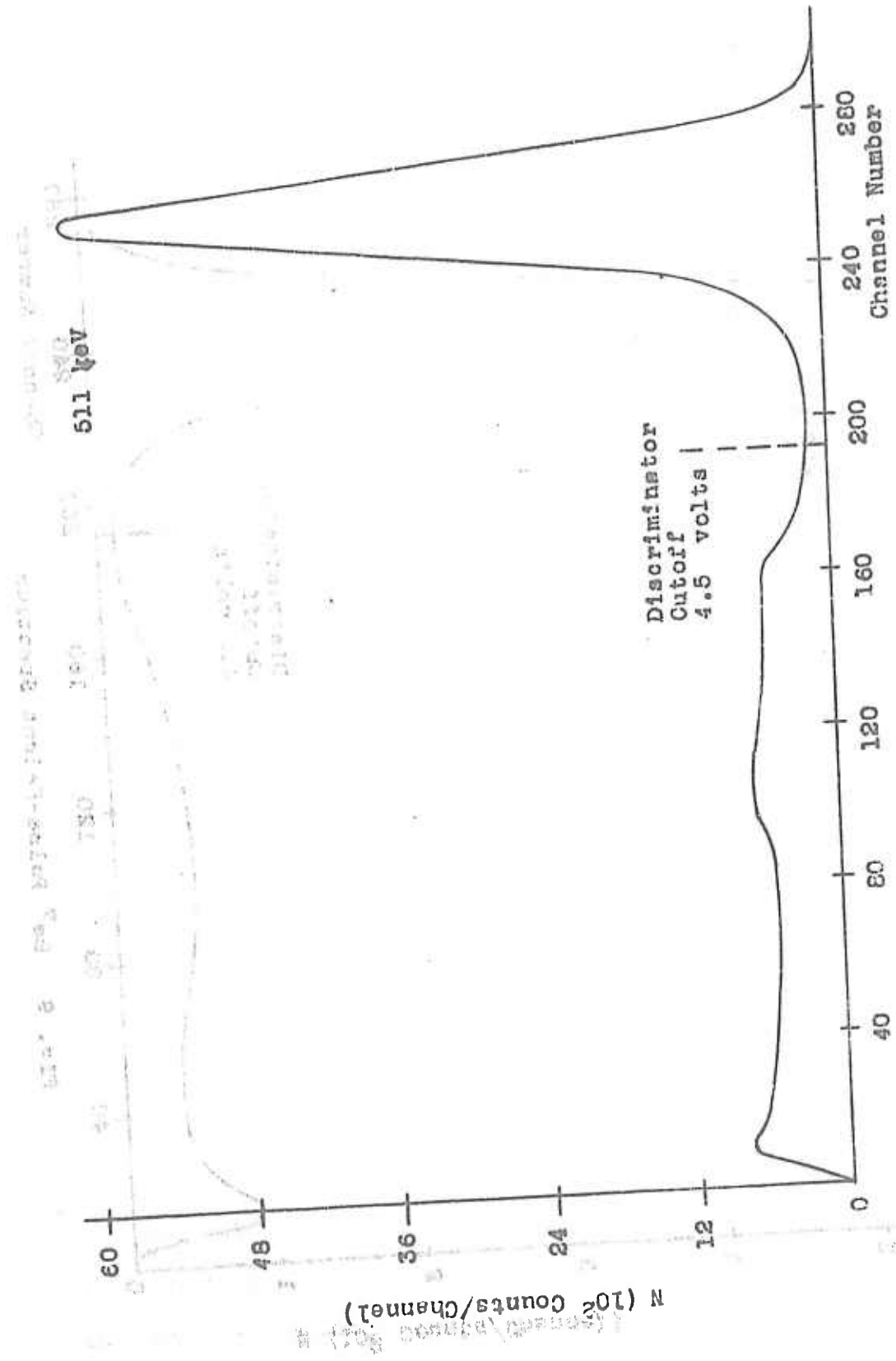


Fig. 8 C11 Pulse-Height Spectrum

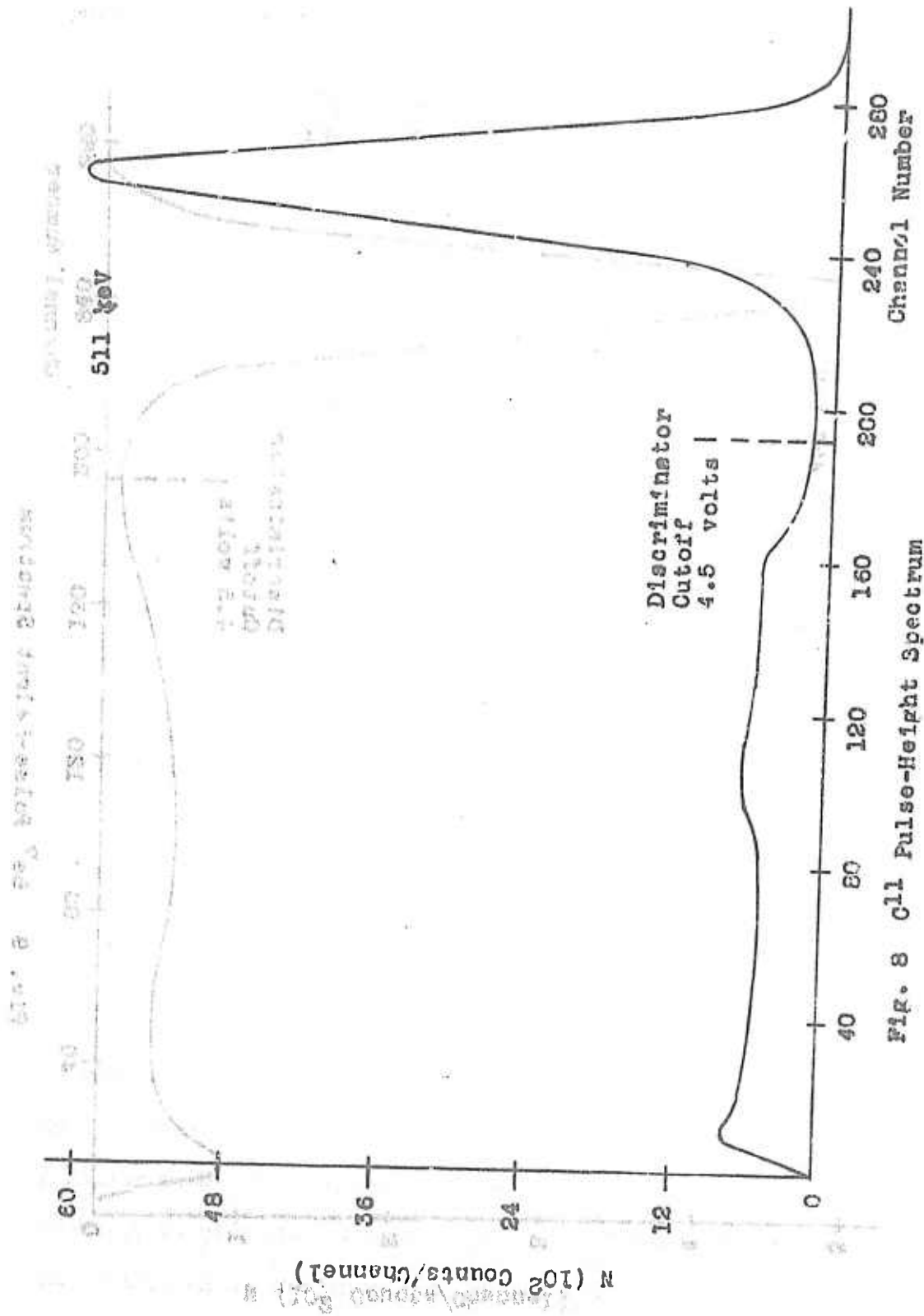


Fig. 8 511 Pulse-Height Spectrum

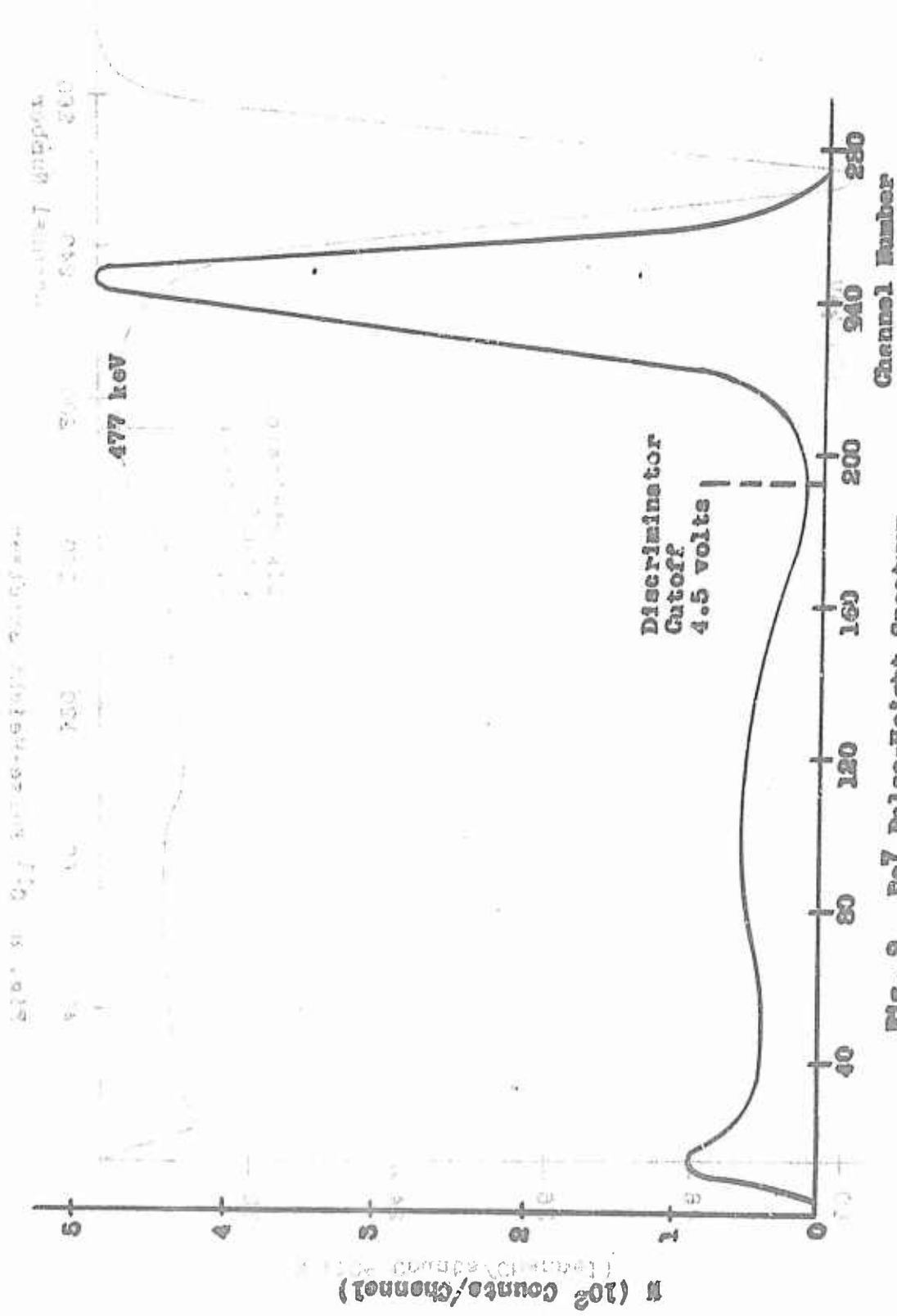


Fig. 9 Be7 Pulse-Height Spectrum

to make a measurement, the remaining N^{13} activity was too weak to be noticed in comparison with the remaining C^{11} activity. In any case, if both N^{13} and C^{11} were present in a given sample, the actual separation of these activities was performed by the computer program.

G. Efficiency of Counting

The counter efficiency was calculated on the basis of purely geometrical considerations using a technique due to Heath [9]. In this method any photon interaction in the counter crystal is assumed to cause a detectable pulse. The stated efficiency is thus a measure of the probability that a photon entering the crystal will cause a pulse somewhere in the spectrum. If, however, only those pulses which are in the photopeak are accepted, as in our case when an integral discriminator was used, a method of determining the ratio of counts under the peak to total counts in the spectrum must be devised. For these "peak-to-total ratios" we simply used the numbers 0.653 for Be^7 and 0.630 for C^{11} obtained from the data of Heath for a source placed 0.5 centimeters from the counter. These ratios were obtained under the conditions of very good geometry (no back-scattering) which also apply to the efficiency calculation.

The total efficiency calculation for a thin disc source on the axis of a cylindrical counter is discussed more fully in Appendix 2. Considering a thick target to be composed of a sum of thin discs, one obtains the following mean efficiencies: 0.287 for the carbon samples, 0.261 for melamine, and 0.257 for water. These are the efficiencies used in our calculations.

We may now assemble the various relevant factors into one expression from which the true activity is to be calculated,

$$A = \frac{A_p}{\epsilon P S} \quad (26)$$

Here A_p is the measured activity in the photopeak (assumed equal to the number of pulses which pass the discriminator in unit time), ϵ is the counter efficiency, P is the peak-to-total ratio, and S corrects for self-absorption in the source. The latter was determined experimentally by measuring the efficiency with carbon discs inserted between a thin Ca^{137} source and the detector. The factor S was found to be no less than 0.975. In addition, for the positron annihilation measurements we divided A by 2 to take into account the fact that two photons are emitted in this process.

H. Calculation of the Activity

The activity of the samples at time t , the instant when irradiation ceased, was obtained from a sequence of activity measurements made at various later times. The raw data of these activities and the times at which they were measured was processed by a computer program designated FRANTIC which was written by Rogers [10] for computers using a FORTRAN compiler. The program corrects the raw data for background activity, counter system dead time, and any uncertainties in these quantities. It then fits one or more exponential decay curves to the corrected activity points by the method of least squares. The decay constant and the initial number of nuclei being the parameters through which the fit is made, these quantities, and the standard deviation of each,

are the output information from the program. For mixtures of simple activities the program fits the longest-lived activity first, progresses to the next longest, and so on, giving values for each of the decay constants and initial activities.

I. Error Analysis

Precise analysis of the errors in the reported quantities presents formidable difficulties; it will not be attempted here. Instead we shall merely summarize the statistical and instrumental uncertainties as we have estimated them.

The activity A_0 , perhaps the most interesting quantity that was measured in the experiment, is known with a reasonable precision. Even so, A_0 involves the statistical uncertainties in the individual counts, mostly less than 0.5 percent, the error in the fit to the data, usually less than 1.0 percent, and the uncertainties in the detector apparatus. Of these, the 5 percent uncertainty in the dead time measurement will contribute a negligible error for most of the measurements. Of more importance, the uncertainty in total efficiency of the counter may be as much as 5 percent, in the peak-to-total ratio about 5 percent, and in the self-absorption factor another 1 percent. Were one to consider these uncertainties as normally distributed (a highly suspect assumption), the total error in A_0 alone would be about 6 percent.

To obtain the cross sections, however, one must know both the amount of material in the beam and the current of bombarding electrons with some precision. For the former, we believe the error made in measuring radiating material and target thickness is

less than 1 percent, except for the melamine target where 5 percent is perhaps more appropriate. The error made by assuming the copper bremsstrahlung spectrum to be valid for all the radiators incorporates perhaps another 1 percent of uncertainty. The determination of the number of bombarding electrons is, however, highly uncertain. In the first place, the absolute efficiency of the secondary-emission monitor is uncertain to about 10 percent. Worse yet, the integrating circuit interposed an intermittent leakage current the magnitude of which was known only to within 20 percent, at best. This gives a total uncertainty of measured charge of as much as 10 percent. Coupled with the uncertainty in the monitor efficiency, this may lead to an error as large as 20 percent in the absolute value of accumulated charge.

When all the uncertainties are added together, by whatever specific technique, it is easy to imagine a total uncertainty of 30 percent in the measurement of a given yield. Since the final cross section calculation involves a difference of yields, however, the error in the cross section for carbon or oxygen may be as large as 50 percent. Still more uncomfortably, the nitrogen calculation involves subtraction of the carbon yield from that for melamine. The error here may be several hundred per cent.

IV. RESULTS

The final cross sections that are reported in this chapter are based on the experimental data set forth in Table II below. The quantity listed in column 3 of the table is the integral stated in the denominator of equation (9) in Chapter III. It is calculated here for the C^{11} measurement only. The uncorrected activities stated in columns 4, 5, and 6 simply list the counting rate at the time the irradiation ceased. These are the raw output data of the computer and are based on the actual counter output corrected only for dead time and background. Other data concerning radiator thicknesses and total accumulated charge were taken from Table I in Chapter II.

TABLE II
Experimental Data

Target	Thickness NT (10^{22} cm $^{-2}$)	Current Integral (10^{16} el)	Uncorrected Activities		
			C^{11} (10^5 ct/s)	Be 7 (ct/s)	N 13 (10^4 ct/s)
Carbon 1	4.00	1.091	60.7	20.3	-
Carbon 2	4.03	0.882	20.3	10.4	-
Carbon 3	4.02	1.010	25.3	14.3	-
Mel. 1	0.263	1.270	17.0	9.48	-
Mel. 2	0.273	0.870	5.16	5.30	-
Water 1	2.22	0.900	0.406	2.69	7.46
Water 2	2.22	1.180	0.221	1.20	4.35

The electromagnetic disintegration cross sections for the formation of the unstable nuclei C^{11} , Be 7 , and N 13 from the various

target nuclei are stated in Tables III, IV, and V, respectively, in units of microbarns. The photodisintegration cross section, σ_a , appearing in the second column of the tables is, of course, the average cross section per equivalent photon. In calculating this quantity, we used the value 67.0 MeV for the integrated photon intensity spectrum arising from electrons of primary energy 75 MeV. From this one obtains on the average 0.894 equivalent photons of energy 75 MeV for each electron that penetrates one radiation length of matter.

TABLE III

Total Cross Section for Formation of C^{11}

Nucleus	$\sigma_a (\mu b)$	$\sigma_b (\mu b)$	σ_a/σ_b
Carbon	823	17.5	47
Nitrogen	133	7.71	17
Oxygen	12.1	0.32	38

TABLE IV

Total Cross Section for Formation of Se^7

Nucleus	$\sigma_a (\mu b)$	$\sigma_b (\mu b)$	σ_a/σ_b
Carbon	68.6	1.30	53
Nitrogen	7.95	1.05	7.6
Oxygen	8.67	0.139	62

TABLE V
Total Cross Section for Formation of N^{13}

Nucleus	$\sigma_a(\mu b)$	$\sigma_a'(\mu b)$	σ_a/σ_e
Oxygen	31.6	0.24	132

One should note that the probable error in these cross sections may well be in excess of 50 percent. It is thus not reasonable to expect detailed agreement between the numbers and any other published results that fall in the same domain. Even so, our results are internally consistent to the extent of displaying proper trends. For example, the cross sections for both types of disintegration processes fall off with increasing Z of the target nucleus. This is to be expected on the general grounds that any particular process has a smaller probability of occurrence when the possible number of processes increases, as in heavier targets. We note also the general consistency among the ratios of photodisintegration to electrodisintegration cross sections for the various nuclear targets.

On the other hand, agreement with the results of other experiments is indeed very poor. The experiment of Barber et al. [13] on the $C^{12}(\gamma, n)C^{11}$ reaction determined the activation cross section to be 2.2×10^{-27} cm² for bombardment with x-rays of 75-MeV maximum energy. This cross section is analogous to our photodisintegration yield, γ_y , for which we found the value 6.5×10^{-28} cm², which differs by a factor of 3.4 from Barber's result. In another experiment involving C^{11} production, Barber [5] found the ratio σ_a/σ_e to have the value 14.4, a factor of 3.3 lower than our result.

In the case of processes leading to the production of Be^7 our results agree but little better with the published values of other groups of experimenters. Artus [4] states that the photodisintegration cross section σ_a for the Be^7 processes out of carbon and oxygen have values of 143 and 12 microbarns, respectively, for x-rays with maximum energy of 55 MeV. Our values for these quantities are lower by factors of about 2 for reasons unknown to us. Our electrodisintegration cross sections for Be^7 processes must, however, stand alone without comparison with other work, as must the nitrogen photodisintegration cross section. No other published results for these quantities are known to us.

In Table VI are listed the equivalent radiator thicknesses X_e which arise from comparison between the effects on the disintegration processes of the real x-ray spectrum and the virtual photon spectrum of the electron fields. The entries in the table seem to be in reasonably good agreement with the approximate theoretical value $X_e = 10 \alpha / \pi = 0.023$ radiation lengths in all cases except that of nitrogen.

TABLE VI
Equivalent Radiator Thicknesses

Nucleus	X_e (radiation lengths)	
	C^{11} process	Be^7 process
Carbon	0.0271	0.0195
Nitrogen	.0108	.1265
Oxygen	.0199	.0216

The large experimental uncertainties in our work, especially that involving nitrogen, make our results only tentative. Nevertheless, we can conclude that Be^7 and C^{11} are produced in some quantity from carbon, nitrogen, and oxygen. Evidence for the production of N^{13} from oxygen is also unambiguous. The experiment must be repeated with greater care, however, before the quantitative results can lend themselves to a meaningful theoretical interpretation.

BIBLIOGRAPHY

1. For photodiintegration results see for example: K. Strauch, *Ann. Rev. Nuclear Sci.* 2, 105 (1953); J. S. Levinger, *Ann. Rev. Nuclear Sci.* 4, 13 (1954); or D. H. Wilkinson, *Ann. Rev. Nuclear Sci.* 9, 1 (1954).
2. W. C. Barber and V. J. Vanhuyse, *Nuclear Phys* 16, 381 (1960).
3. F. K. Goward and J. J. Wilkins, *Proc. Roy. Soc. (London)* 228 A, 376 (1955).
4. H. Artus, *Z. Physik* 189, 355 (1966).
5. W. C. Barber, *Phys. Rev.* 111, 1642 (1958).
6. W. Heitler, *The Quantum Theory of Radiation Third Ed.* (Oxford University Press, 1954), p. 247.
7. H. W. Koch and J. W. Motz, *Rev. of Mod. Phys.* 31, 920 (1959).
8. H. A. Bethe and J. Ashkin, *Experimental Nuclear Physics* (John Wiley and Sons, Inc., New York, 1953), I, p. 266.
9. R. L. Heath, *Scintillation Spectrometry Gamma-Ray Spectrum Catalog*, AEC Report IDO-16408 (1957).
10. P. C. Rogers, *FRANTIC Program for Analysis of Exponential Growth and Decay Curves*, M.I.T. Tech. Report No. 76 (1962).
11. T. Lauritsen and F. Ajzenberg-Selove, *Nuc. Phys.* 78, 1 (1966).
12. G. R. White, *X-ray Attenuation Coefficients from 10 Kev to 100 Mev*, Natl. Bur. Standards Report 1003 (1952).
13. W. C. Barber, W. D. George, and D. D. Reagan, *Phys. Rev.* 98, 73 (1955).

APPENDIX I

We shall here describe a few aspects of the electronic circuits named in the block diagram of Fig. 4 in Chapter II. Pulses of light from the NaI crystal are registered in a ten-stage RCA 8054 photomultiplier tube which is connected to the voltage-divider network shown in Fig. 10 below. The circuit was designed to provide negative voltage pulses having a fall-time of about 200 microseconds when the device is used in conjunction with an Ortec Model 113 preamplifier with a 500 picofarad input capacitor. Such pulses have an optimum duration for linear amplification by the Ortec Model 410 amplifier to which they are led.

Output pulses from the linear amplifier are bipolar, having positive and negative amplitudes in the range 0 to 10 volts. These pulses are analyzed either by the Nuclear Data Model 180 512-channel analyzer or by the Ortec Model 420 timing single-channel analyzer. In the former case the pulse-height analysis data are stored in the memory unit of the analyzer. These data, in the form of counts per channel, are then available in an oscilloscope display or in printed form from a teletype printer.

Most of the data accumulated in the experiment, however, are the scaled record of voltage pulses which merely had an amplitude larger than a certain minimum. In this case the Ortec 420 single-channel analyzer discriminated between pulses of different amplitudes, accepting only those greater in amplitude than E , the voltage of the integral discriminator setting. The output of the analyzer is a 5-volt, 0.5 microsecond long, rectangular pulse for each accepted input pulse. These pulses are then amplified to a height of 15 volts

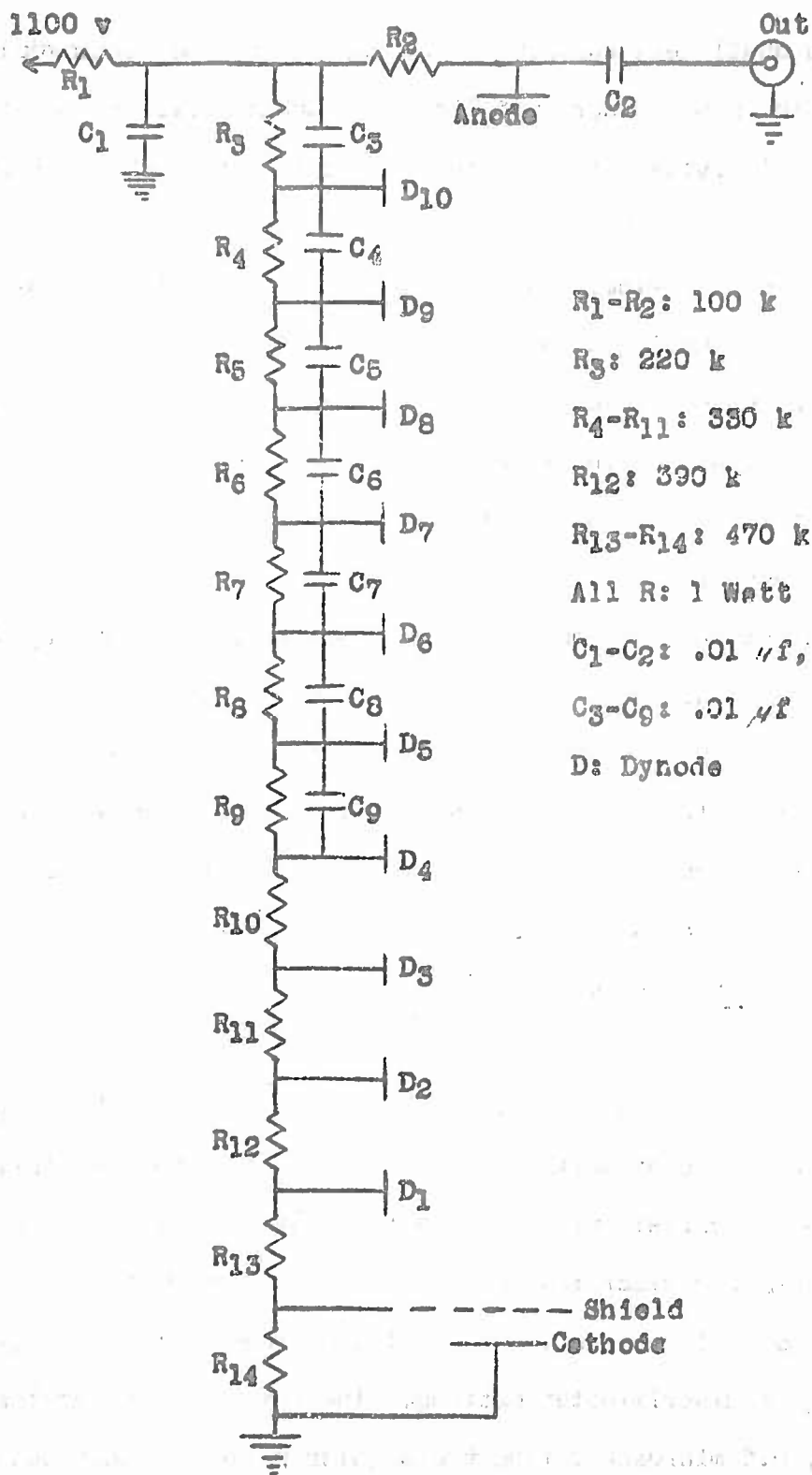


Fig. 10 Photomultiplier Tube Base Circuit

by means of a solid-state amplifier designed and built in this laboratory. The resulting pulses are led to the multi-channel scaling (MCS) input terminals of the Nuclear Data 180. Here the pulses are accumulated in a given one of the available 512 channels of the analyzer. In this mode of use, the MCS mode, the analyzer accepts and registers in the selected channel all the pulses having an amplitude of 15 volts. When counting into one or more channels has been completed, the information in the various channels of the memory is available through the output devices mentioned before.

Selection of the particular channel used for storage is accomplished sequentially by a timing circuit operating with the trigger circuit shown in Fig. 11. The timing circuit determines the dwell time in a given channel. This is done by counting a predetermined number of 60-Hz, 115-volt line pulses by means of a Technical Associates Model DS-58 scaler used in its "Test" mode. When the selected number of pulses has been counted, the scaler output terminal voltage undergoes a step change of -80 volts, which fires the trigger circuit, causing it to send an 8-volt pulse to the EXT IS terminals of the multi-channel analyzer. This causes the analyzer to scale the ensuing input pulses into the next channel in sequence. The output voltage of the scaler then returns to its original level prior to commencement of the next cycle.

The trigger circuit itself (see Fig. 11) operates through the breakdown of the trigger device T caused by a sudden voltage drop at the start switch or at the input terminals. The device T then acts as a short circuit, permitting capacitor C to discharge through resistor R, and resulting in the desired 8-volt output pulse.

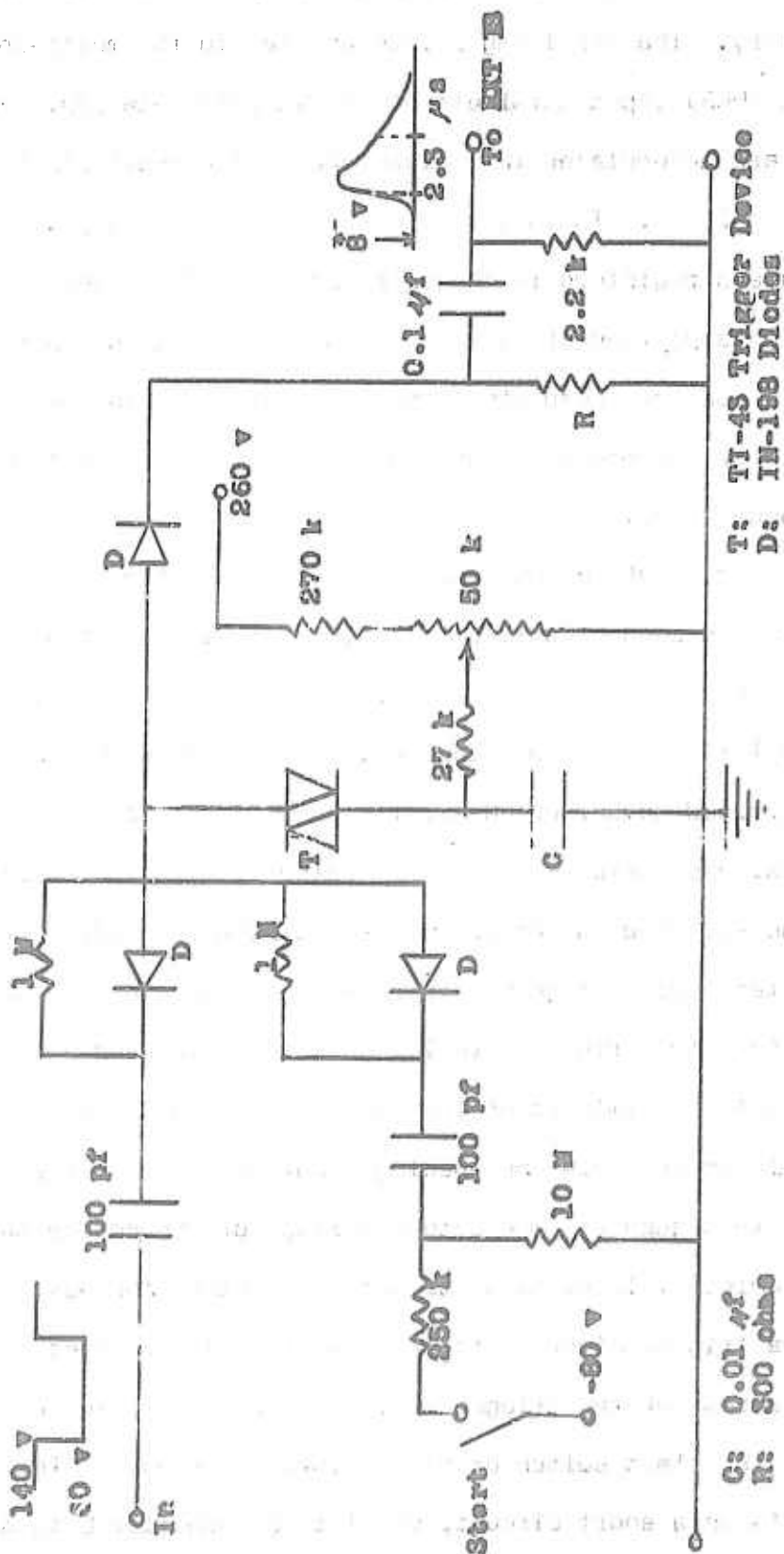


Fig. 11 Channel Advance Trigger Circuit

T: TI-4S Trigger Device
D: IN-198 Diodes

C: 0.01 μf
R: 500 ohms

APPENDIX II

Efficiency Determination

The calculation of the absolute efficiency of photon detection for a disc source on the axis of a cylindrical crystal can be made very accurately from purely geometrical considerations. The method effectively determines the joint probability that a photon will be intercepted by the crystal and will have some kind of interaction in the crystal material. For the counter efficiency in this experiment we performed a numerical integration of the equation presented by Heath [9] as follows:

$$\epsilon(k) = \frac{1}{\pi R^2} \int_0^R x dx \int_{-\frac{\pi}{2}}^{\frac{\pi}{2}} d\phi \left\{ \int_0^{\tan^{-1}(\frac{B}{h_0+t_0})} \left[1 - e^{-\tau(k) \frac{t_0}{\cos \theta}} \right] \sin \theta d\theta \right. \\ \left. + \int_{\tan^{-1}(\frac{B}{h_0+t_0})}^{\tan^{-1}(\frac{B}{h_0})} \left[1 - e^{-\tau(k) \left(\frac{B}{\sin \theta} - \frac{h_0}{\cos \theta} \right)} \right] \sin \theta d\theta \right\}, \quad (27)$$

where

$$B = -x \sin \phi + \left[x^2 \sin^2 \phi + r_0^2 - x^2 \right]^{1/2}$$

The square-bracket expressions in the integrals state the probability that the photon of energy k will have an interaction when it impinges on a thickness of material equal to the factor which multiplies the absorption coefficient $\tau(k)$ in the exponentials. The quantities R and r_0 are radii of the disc and counter, respectively, t_0 is the

crystal length, h_0 is the distance from the disc to the crystal face, θ and ϕ are angular variables of integration, and x the variable by means of which integration over the disc is achieved. Values of the x-ray absorption coefficients $\mu(k)$ for NaI(Tl) that we used in the calculation were taken from the work of G. R. White [12].

Since the sources used in the experiment were relatively thick, we found it necessary also to carry out an integration over the source thickness in the efficiency calculation. In practice, this was actually done by calculating the thin-disc efficiency for the two ends and the mid-plane of the cylindrical source. We then integrated the results by using the Simpson three-point formula. The results of these calculations for the three different source types used in the experiment are given in Table VII for which we determined source radii according to the following considerations. Since the accelerator beam spot was one-half inch in diameter, the carbon disc received the greater portion of its irradiation in the central one-half inch; thus the largest percentage of the detectable gammas originate in this part. For the carbon calculation, then, the radius of the carbon discs was assumed to be 0.250 inches. For the water and melamine samples, however, the disc radius was assumed equal to the bottle radius, 0.485 inches.

TABLE VII
Detector Efficiency

<u>Sample</u>	<u>h_0 (inches)</u>	<u>Efficiency for disc at h_0</u>	<u>Mean Efficiency</u>
CARBON	0.133	0.32488	0.28710
	0.233	0.28597	
	0.333	0.25382	
MELAMINE	0.133	0.32060	0.26099
	0.305	0.25824	
	0.477	0.21237	
WATER	0.133	0.32060	0.25667
	0.321	0.25353	
	0.508	0.20529	

UNCLASSIFIED
Security Classification

DOCUMENT CONTROL DATA - R&D

(Security classification of title, body of abstract and indexing annotation must be entered when the overall report is classified)

1. ORIGINATING ACTIVITY (Corporate method) Ordnance Engineering Programs Naval Postgraduate School		2a. REPORT SECURITY CLASSIFICATION Unclassified	
		2b. GROUP	
3. REPORT TITLE The Production of Be^7 and C^{11} from Carbon, Nitrogen, and Oxygen by 75-MeV Electrons			
4. DESCRIPTIVE NOTES (Type of report and inclusive dates) Thesis			
5. AUTHOR(S) (Last name, first name, initial) James H. Lusk, Major, USA Glenn W. Pomykal, LT., USN			
6. REPORT DATE June 1967		7a. TOTAL NO. OF PAGES 53	7b. NO. OF REFS 13
8a. CONTRACT OR GRANT NO.		8b. ORIGINATOR'S REPORT NUMBER(S)	
a. PROJECT NO.			
c.		9d. OTHER REPORT NO(S) (Any other numbers that may be assigned to report)	
d.			
9c. AVAILABILITY/LIMITATION NOTICES This document is subject to special export controls and each transmittal to foreign governments or foreign nations may be made only with prior approval of the Naval Postgraduate School.			
11. SUPPLEMENTARY NOTES		12. SPONSORING MILITARY ACTIVITY	
13. ABSTRACT An investigation was made of the electromagnetic disintegration of carbon, nitrogen, and oxygen leading to production of the unstable nuclei Be^7 and C^{11} . Targets of graphite, melamine, and water were bombarded with 75-MeV electrons from the Naval Postgraduate School linear accelerator. The disintegration fragments of interest were counted by detecting their decay activity, Be^7 by the 477-Kev gamma ray from its daughter nucleus and C^{11} by the 511-Kev photons from the annihilation of its emitted positron. Electron and photon effects were separated by interposing an additional radiator for one bombardment of a given type of target, then repeating with a similar target without the radiator. Radioactive fragments of Be^7 and C^{11} were found in all bombardments; N^{13} was also found in bombardments of melamine and water. Electrodisintegration cross sections for processes yielding C^{11} were found to range from $17.5 \mu b$ for carbon down to $0.3 \mu b$ for oxygen. The corresponding values for processes yielding Be^7 ranged from $1.3 \mu b$ to $0.14 \mu b$. Integrated photodisintegration cross sections were found to be approximately 50 times greater than these.			

DD FORM 1473
1 JAN 63

UNCLASSIFIED
Security Classification

